Volume 18, Number 4, 2025. pp. 467-475

Jordan Journal of Physics

ARTICLE

Charge Density Distributions for Elastic and Inelastic Longitudinal Electron Scattering Form Factors of ^{28}Si and ^{32}S Nuclei

H. K. Issa and **Ghaith N. Flaiyh**

Department of Physics, College of Science, University of Baghdad. Baghdad, Iraq.

Doi: **https://doi.org/10.47011/18.4.5**

Received on: 05/06/2024; *Accepted on: 06/10/2024*

Abstract: The charge density distributions were calculated using the folding model, which was applied to study the roles of center-of-mass motion and Pauli pair association affecting the density dependence of effective two-body interactions. A formula for the two-body density applicable to light nuclei was derived in terms of the pair correlation function. For ^{28}Si and ^{32}S, the elastic electron-scattering form factors F(q) and the root-mean-square charge radii $\langle r^2\rangle^{(1/2)}$ were determined. The inelastic longitudinal electron scattering form factors associated with the isosceles transitioning T = 0 of the $(0^+ \rightarrow 2^+),(0^+ \rightarrow 2_1^+), 0^+ \rightarrow 4_1^+)$ for the ^{28}Si and ^{32}S nuclei were determined. A wave function within the model space defined by the orbits $1d_{5/2}$ $1d_{5/2}$, $2s$ $s_{1/2}$, and $1d_{3/2}$ was found to be insufficient to produce an acceptable form factor. The core-polarization impacts were assessed by incorporating the Tassie-model shape and the two-body charge density distributions into the model space, which resulted in a high degree of matching with the experimental data.

Keywords: Charge density, Elastic electron scattering, Tassie-model, Form factor and interactions.

PACS numbers: 21.30.Fe., 21.60.-n.

1. Introduction

Electron scattering is the consequence of an electromagnetic interaction. There is a multitude of theories that consider an electron as an effective instrument for the study of the structure of nuclear particles [1, 2]. The electron's fundamental attachment to the object that can be used as a targeted nucleus is well-established. It is feasible to conduct measures on the targeted nucleus without substantially altering its structure as a result of the relatively faint interaction. However, the target's shape and its relationship to nuclear particles are not known. This makes it very difficult to make distinctions between them during the examination of the results of experiments. The effect of the electron-scattering operator instantly links its cross-section to the change in the matrix components of the localized charge and current-density operator, which, in turn, is directly related to the target nucleus's structure [3].

Radhi *et al.* [4] studied the nuclear structure of ^{19}F nucleus using inelastic electron-scattering form factors, energy levels, and transition probabilities for positive and negative low-lying states. Mahmood and Flaiyh [5, 6] employed an effective two-body density operator for a point-nucleon system folded with the tensor-force correlations. The operator was used to derive an explicit form for the ground-state two-body charge density distribution (TBCDD) applicable to some light nuclei.

Sarriguren *et al.* [7] studied magnetic form factors corresponding to elastic electron scattering from odd-A nuclei using the plane-wave Born approximation.

Al-Rahmani *et al.* [8] studied short-range effects on the longitudinal Coulomb form factors C2, C3, and C4 in the ^{26}Mg nucleus. Flaiyh and

Corresponding Author: H. K. Issa **Email**: hassan.kalid@sc.uobaghdad.edu.iq

Sharrad [9] studied the effective two-body density operator for a point-nucleon system folded with the full two-body correlations (which include the tensor correlations and short-range correlations).

The folding model has proven highly effective for the phenomenology examination of nucleon-nucleus. In this approach, the scattering results are obtained using the ground-state density of the target nucleus and an effective two-body interaction [10]. In the model's initial applications, the objective density was thought to be unrelated to the effective interaction.

In this work, charge density distributions as well as elastic and inelastic form factors were investigated for the ^{28}Si and ^{32}S target nuclei. It has been previously acknowledged that electron-scattering data are inadequately described when form factors are calculated exclusively using the extensive particle-shell model space.

Thus, it has become imperative to include the consequences for the two-body effective folding model (core polarization) in the equations. This phenomenon can be attributed to the polarization of core protons by ligand protons and neutrons. The gamma-transition and the excited state of nuclei through electron-scattering have been described using the Tassie model. It is the multipole analysis of inelastic scattering. This model is limited to the standard liquid drop model when a uniform charge distribution is assumed. The Tassie model is an attempt to develop a model that is more elastic and can be modified to accommodate a non-uniform charge and mass density distribution. The density of the core-polarization transformation is contingent upon the nucleus's ground state charge density, as per this model. The ground charge density is expressed according to the two-body charge density distributions across all occupied shells, which includes the core. The Tassie model [11] provides the shape of the transition density for the excitation in question. This model, when coupled with the two-body charge density distribution and simple shell model predictions, results in a high degree of accord in both the evaluated and observed data for the longitudinal structure factors of elastic and inelastic materials during transitions $J_i\ T_i \rightarrow J_f\ T_f\ 0+\ 0 \rightarrow 2_1^+\ 0$ and $4_1^+\ 0$ for ^{28}Si and ^{32}S nuclei.

2. Theoretical

The charge density of a nucleus composed of A particles that are shaped like points is expressed by the following operator equation [12]:

$$\rho_{ch}^{(1)}(\mathrm{r}) = \frac{1}{4\pi}\sum_{n\ell j}\eta_{n\ell j}(2j+1)\left|R_{n\ell}(\mathrm{r})\right|^2 \qquad (1)$$

where the state's livelihood percentage is represented by the parameter $\eta_{n\ell j}$, $R_{n\ell}(r)$ is the harmonic oscillator radial wave function, and (2j+1) is the occupation number of sub–orbits.

The pair-correlation function can be used to determine an equation for the density of two-body operators that are suitable for finite nuclei, based on the following relation:

$$\rho^{(2)}{}_{(\vec{r}1,\vec{r}2)} = \rho^{(1)}(\vec{r}_1)\,\rho^{(1)}(\vec{r}_2) + C(\vec{r}_1,\vec{r}_2) \qquad (2)$$

$C(\vec{r}_1,\vec{r}_2)$ is the center of mass $C_{cm}(\vec{r}_1,\vec{r}_2)$ and Pauli pair-correlation functions $C_p(\vec{r}_1,\vec{r}_2)$, respectively [13]. That is:

$$C(\vec{r}_1,\vec{r}_2) \cong C_{c.m.}(\vec{r}_1,\vec{r}_2) + C_p(\vec{r}_1,\vec{r}_2) \qquad (3)$$

where, according to Ref. [13]:

$$C_{c.m.}(\vec{r}_1,\vec{r}_2) = \frac{r_1 r_2}{2A\alpha^2}\left(\frac{1}{r_1}\frac{d\rho_1}{dr_1}\right)\left(\frac{1}{r_2}\frac{d\rho_1}{dr_1}\right) \qquad (4)$$

$$C_{p_{(\vec{r}_1,\vec{r}_2)}} \cong \frac{1}{A-1}\left[1 - \frac{c_0}{A-1}e^{\frac{K_f^2}{5}|\vec{r}_1-\vec{r}_2|^2}\right]\rho^{(1)}$$

$$C_p(\vec{r}_1,\vec{r}_2) \cong \frac{1}{A-1}\left[1-\frac{c_o}{A-1}e^{\frac{k_f^2}{5}|\vec{r}_1-\vec{r}_2|}\right] \qquad (5)$$

$$\rho^{(1)}{}_{(\vec{r}_1)}\rho^{(1)}{}_{(\vec{r}_2)}.$$

where $c_o = 3(\pi/5)^{1/2}$, α is the oscillator constant $\left(\alpha^2 = 0.99\,A^{-1/3}\right)$, and k_f is the local Fermi momentum.

By substituting Eqs. (4) and (5) into Eq. (3), and then using Eq. (3) in Eq. (2), we get:

$$\rho^{(2)}(\vec{r}1,\vec{r}2) = \rho^{(1)}(\vec{r}1)\rho^{(1)}(\vec{r}2) + \frac{r_1 r_2}{2A\alpha^2}\left(\frac{1}{r_1}\frac{d\rho_1}{dr_1}\right)\left(\frac{1}{r_2}\frac{d\rho_1}{dr_1}\right) + \rho^{(2)} \quad \frac{1}{A-1}\left[1-\frac{c_0}{A-1}e^{\frac{k_f^2}{5}|\vec{r}1-\vec{r}2|}\right]. \quad (6)$$
$$\rho^{(1)}(\vec{r}_1)\,\rho^{(1)}(\vec{r}_2)$$

The ground-state for a two-body charge density distribution, $\rho_{ch}^{(2)}(r)$, is given by the expected result for the functional two-body charge density distribution generator given in Eq. (6), which can be rewritten as

$$\rho_{ch}^{(2)}(r) = \sum_{i<j}\langle ij|\rho_{(r_i,r_j)}^{(2)}[|ij\rangle - |ji\rangle] \quad (7)$$

where $|ij\rangle$ is the two-particle wave function.

The root-mean-square charge radius for nuclei is based on the following relation:

$$\langle r^2\rangle^{1/2} = \frac{4\pi}{z}\int_0^\infty \rho_{ch}(r)\,r^4 dr \quad (8)$$

The ground-state charge density distribution can be utilized to compute the elastic electron-scattering form factors for spin-zero nuclei such as ^{28}Si and ^{32}S. All coming and scattered waves of electrons are approximated as plane waves according to the plane wave Born approximation (PWBA), where the ground-state charge density distribution is real and spherically symmetric. Consequently, the form factor is simply the Fourier transform of the ground-state charge density distribution [14, 15]:

$$F(q) = \frac{4\pi}{Z}\int_0^\infty \rho_o(\mathrm{r})\,j_0(qr)\,\mathrm{r}^2 d\mathrm{r} \quad (9)$$

where $\rho_{o\,(r)}$ $\rho_0(r)$ is the ground-state two-body charge density distribution defined in Eq. (7), and $j_0(qr) = \sin(qr)/(qr)$ $j_0(qr) = sin(qr)\ /(qr)$ is the zeroth order of the spherical Bessel function. Here, q represents the momentum transferred from the incident electron to the target nucleus. It is possible to express Eq. (9) as:

$$F(q) = \frac{4\pi}{qZ}\int_0^\infty \rho_o(\mathrm{r})\sin(qr)\,\mathrm{r}dr \quad (10)$$

The form of the factors of inelastic longitudinal electron scattering, which involves angular momentum J and momentum transfer, is expressed as [11]:

$$\left|F_J^L(q)\right|^2 = \frac{4\pi}{Z^2(2J_i+1)}\left|\left\langle f\left\|\hat{T}_J^L(q)\right\|i\right\rangle\right|^2 \left|F_{cm}(q)\right|^2\left|F_{fs}(q)\right|^2. \quad (11)$$

where $\hat{T}_J^L(q)$ $\hat{T}_J^L(q)$ is the longitudinal electron-scattering generator. Consequently, the form factors in Eq. (11) can be expressed in terms of matrix elements that are decreased in both angular momentum and isospin, as the nuclear states have clearly established isospin $T_{i/f}$ [16]. Alternatively:

$$\left|F_J^L(q)\right|^2 = \frac{4\pi}{Z^2(2J_i+1)}\left|\sum_{T=0,1}(-1)^{T_f-T_{z_f}}\begin{pmatrix} T_f & T & T_i \\ -T_{Z_f} & 0 & T_{Z_i}\end{pmatrix}\left\langle f\left\|\hat{T}_{JT}^L(q)\right\|i\right\rangle\right|^2 \left|F_{cm}(q)\right|^2\left|F_{fs}(q)\right|^2 \quad (12)$$

where $T\,T$ is constrained by the subsequent selection rule:

$$\left|T_f - T_i\right| \le T \le T_f + T_i \quad (13)$$

with $T_z = (Z-N)/2$. The bracket $\begin{pmatrix} & \end{pmatrix}$ in Eq. (12) is the 3–*j* symbol. The decreased matrix elements in spin and isospin space of the longitudinal operator between the final and initial plurality of particle states of the structure, such as the arrangement of mixing, are expressed as a function of the one-body density matrix (OBDM) elements produced by the single-particle matrix elements of the longitudinal operator [17] as:

$$\left\langle f\left\|\hat{T}_{JT}^L\right\|i\right\rangle = \sum_{a,b} OBDM^{JT}(i,f,J,a,b)\left\langle b\left\|\hat{T}_{JT}^L\right\|a\right\rangle \quad (14)$$

Additionally, the longitudinal operator's numerous particle-reduced matrix components include two components: one for the model space and the other for the core polarization matrix element [18]. Thus:

$$\langle f\| \hat{T}_J^L(\tau_Z,q)\|i\rangle = \left\langle f\left\| \hat{T}_J^{L,ms}(\tau_Z,q)\right\| i\right\rangle + \left\langle f\left\| \hat{T}_J^{L,cor}(\tau_Z,q)\right\| i\right\rangle$$

$$\left\langle f\| \hat{T}_J^L(\tau_Z,q)\|i\right\rangle = \left\langle f\left\| \hat{T}_J^{L,ms}(\tau_Z,q)\right\| i\right\rangle + \left\langle f\left\| \hat{T}_J^{L,cor}(\tau_Z,q)\right\| i\right\rangle. \quad (15)$$

which is the model-space matrix element in Eq. (15), which can be written as

$$\left\langle f\left\| \hat{T}_J^{L,ms}(\tau_Z,q)\right\| i\right\rangle = e_i \int_0^\infty dr\, r^2 j_J(qr)\, \rho^{ms}_{J,\tau_Z}(i,f,r) \quad (16)$$

The model-space transition density is $\rho_J^{ms}(i,f,r)$. This sum is calculated as the product of the OBDM and the single-particle matrix components, and it is denoted by [3]:

$$\rho^{ms}_{J,\tau_Z}(i,f,r) = \sum_{jj'(ms)}^{ms} OBDM(i,f,J,j,j',\tau_z) \left\langle j\|Y_J\|j'\right\rangle R_{nl}(r)\, R_{n'l'}(r) \quad (17)$$

The core-polarization matrix element in Eq. (15) takes the following form [14, 15]:

$$\left\langle f\left\| \hat{T}_J^{L,cor}(\tau_Z,q)\right\| i\right\rangle = e_i \int_0^\infty dr\, r^2 j_J(qr)\, \rho^{core}_J(i,f,r). \quad (18)$$

Here, ρ_J^{core} is the core-polarization transition density, which is contingent upon the model used for core polarization. To account for the effects of core polarization within the model space, the collective modes of the nuclei are represented by the core-polarization transition density, which complements the model-space transition density. The total transition density is calculated using:

$$\rho_{J\tau_Z}(i,f,r) = \rho^{ms}_{J\tau_Z}(i,f,r) + \rho^{core}_{J\tau_Z}(i,f,r) \quad (19)$$

The core-polarization transition density is determined by the Tassie form, as per the collective modes of nuclei [19]:

$$\rho^{core}_{Jt_z}(i,f,r) = N\frac{1}{2}(1+\tau_z)\, r^{J-1}\frac{d\rho_o(i,f,r)}{dr} \quad (20)$$

which represents the base state two-body charge density distribution, as expressed in Eq. (6), and includes a proportionality constant N. The Coulomb form factor for this model is as follows [18]:

$$F_J^L(q) = \sqrt{\frac{4\pi}{2J_i+1}}\ \frac{1}{Z}\left\{\int_0^\infty r^2 j_J(qr)\ \rho_J^{ms}(i,f,r)\ dr + N\int_0^\infty dr\, r^2\, j_J(qr)\, r^{J-1}\ \frac{d\rho_o(i,f,r)}{dr}\right\} F_{cm}(q)\ F_{fs}(q) \quad (21)$$

The radial integral $\int_0^\infty dr\ r^{J+1} j_J(qr)\frac{d\rho_o(i,f,r)}{dr}$ can be expressed as:

$$\int_0^\infty \frac{d}{dr}\left\{r^{J+1} j_J(qr)\,\rho_o(i,f,r)\right\}dr - \int_0^\infty dr\ (J+1) r^J j_J(qr)\rho_o(i,f,r) - \int_0^\infty dr\ r^{J+1}\frac{d}{dr} j_J(qr)\rho_o(i,f,r). \quad (22)$$

In Eq. (22), the initial term contributes zero, while the second and third terms can be joined to give:

$$-q\int_0^\infty dr\, r^{J+1}\rho_o(i,f,r)\left[\frac{d}{d(qr)}+\frac{J+1}{qr}\right] j_J(qr) \quad (23)$$

Based on the recursion link of the spherical Bessel function [19]:

$$\left[\frac{d}{d(qr)}+\frac{J+1}{qr}\right] j_J(qr) = j_{J-1}(qr) \quad (24)$$

Hence,

$$\int_0^\infty dr\ r^{J+1} j_J(qr)\frac{d\rho_o(i,f,r)}{dr} = -q\int_0^\infty dr\, r^{J+1}\ j_{J-1}(qr)\rho_o(i,f,r) \quad (25)$$

Using Eqs. (21)-(25), the form factor may have the form:

$$F_J^L(q) = \left(\frac{4\pi}{2J_i+1}\right)^{1/2}\frac{1}{Z}\left\{\begin{array}{l}\int_0^\infty r^2 j_J(qr)\,\rho^{ms}_{Jt_z}\,dr - \\ Nq\int_0^\infty dr\, r^{J+1}\rho_o(i,f,r)\, j_{J-1}(qr)\end{array}\right\} F_{cm}(q)\, F_{fs}(q) \quad (26)$$

The constant of proportionality N may be identified by evaluating the form of the factor for $q=k$, resulting in the following expression:

$$N=\frac{\int_0^\infty d\mathrm{r}^2 j_J(k\mathrm{r})\rho^{ms}_{J_{T_Z}}(i,f,\mathrm{r})-F_J^L(k)Z\sqrt{\frac{2J_i+1}{4\pi}}}{k\int_0^\infty d\mathrm{r}\,\mathrm{r}^{J+1}\rho_o(i,f,\mathrm{r})j_{J-1}(k\mathrm{r})} \quad (27)$$

The transition amplitude for photon interaction at $q=k$, $B(CJ)$ as:

$$B(CJ)=\frac{[(2J+1)!!]^2\,Z^2\,e^2}{4\pi\,k^{2J}}\left|F_J^L(k)\right|^2 \quad (28)$$

The transitional amplitude $B(CJ)$ is correlated with its form factor.

$$N=\frac{\int_0^\infty dr r^2 j_J(kr)\rho^{ms}_{J_{T_z}}(i,f,r)-\sqrt{\frac{(2J_i+1)B(CJ)}{(2J+1)!!}}k^J}{k\int_0^\infty dr r^{J+1}\rho_o(i,f,r)j_{J-1}(kr)} \quad (29)$$

This is the coefficient of proportionality for open (closed) shell nuclei, which can be established by incorporating the measured reduced transitional amplitude $B(CJ)$ using Eq. (29).

3. Results and Discussion

Figures 1 and 2 illustrate the ground state charge density distributions (in fm^{-3}) in relation to r (in fm) for ^{28}Si and ^{32}S nuclei, respectively. Spreadsheet (1) contains all the parameters necessary for the calculations, including the dimension parameter of the harmonic oscillator (b). The occupancy probabilities (η_{nlj}) of the states are shown in Figs. (1) and (2), which illustrate the charge density distribution. The blue dash is the one-body charge density distribution without correction which depends on Eq. (1), the solid blue line is the two-body charge density distribution, while the black (•) "dotted symbols" are the measured data [20, 21], in units of (fm^{-3}).

Spreadsheet (1) summarizes the variables and parameters employed in the present calculations.

TABLE 1. Spreadsheet (1) of parameters used in the calculation.

^{32}S	^{28}Si	Nuclei
1.91	1.644	b
0.315	0.329	$\alpha^2\,(fm^{-2})$
1	1	$\eta_{1s_{\frac{1}{2}}}$
1	1	$\eta_{1p_{\frac{3}{2}}}$
1	1	$\eta_{1p_{\frac{1}{2}}}$
1	0.8333	$\eta_{1d_{\frac{5}{2}}}$
0.5	0.5	$\eta_{2s_{\frac{1}{2}}}$
0.25	0	$\eta_{1d_{\frac{3}{2}}}$
3.282	3.14	$\langle \mathrm{r}^2\rangle^{1/2}_{\mathrm{theo.}}$
3.239	3.085	$\langle \mathrm{r}^2\rangle^{1/2}_{\mathrm{exp.}}$ [20]

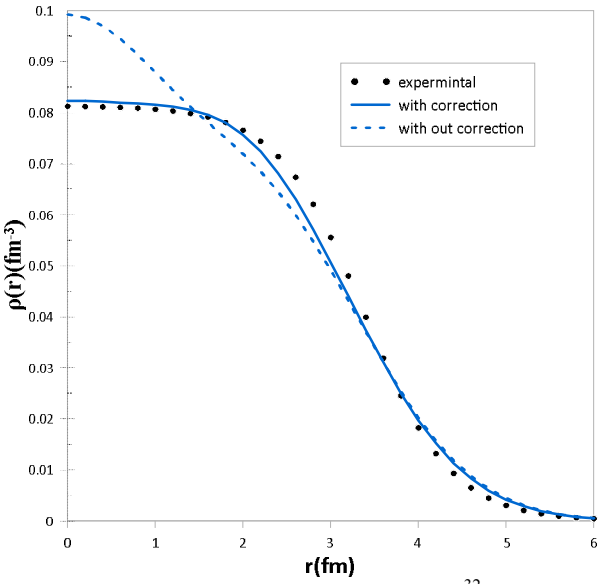

FIG. 2. Charge density distribution for the ^{32}S nucleus.

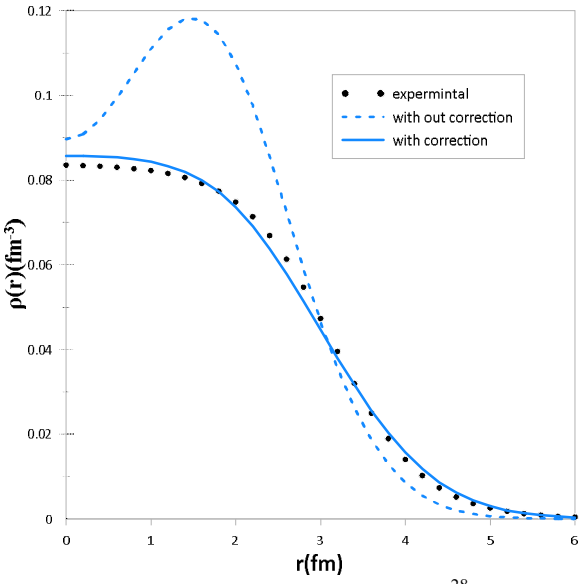

FIG. 1. Charge density distribution for the ^{28}Si nucleus.

As shown in Figs. 1 and 2, the theoretical results exhibit very good agreement with experimental data compared to the two-body charge density distribution in the region 0.5<r <2.5 due to the reduction of the hard-core effects in two-body correlations (center of mass and Pauli pair correlations). The comparison between the one-body and two-body charge density distributions demonstrates that the two-body formulation (solid line) provides a significantly better fit to the experimental data within this region.

The calculated elastic electron scattering form factors F(q) are plotted in Figs. 3 and 4, the calculated F(q)'s are limited to those of experimental data for the ^{28}Si and ^{32}S nuclei, where the blue dash is the elastic form factors without correction using Eqs. (1) and (10). The solid blue line is the two-body elastic form factors with the correction using Eqs. (7) and (10). The black (•) "dotted symbols" are the experimental data in these figures. The calculated F(q)'s are plotted as a function of q, as shown in Figs. 3 and 4. When the two-body charge density distribution is included, a second diffraction minimum appears at q = 2.4, consistent with the experimental observations. This indicates that incorporating two-body correlations yields results that closely match the measured elastic form factors.

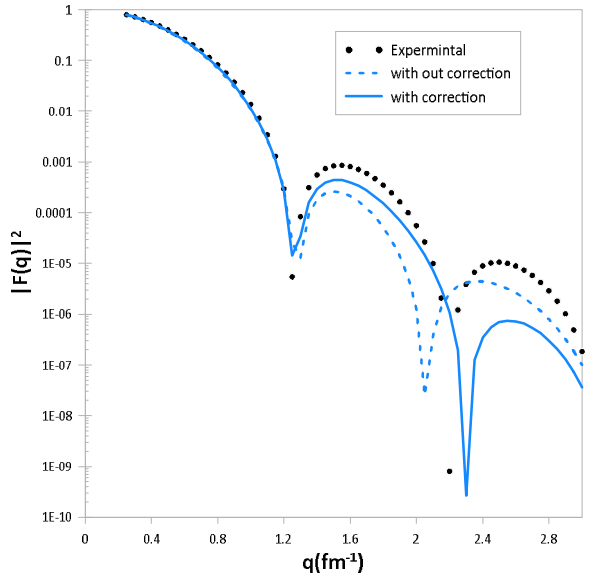

FIG. 4. The elastic form factors for the ^{32}S nucleus.

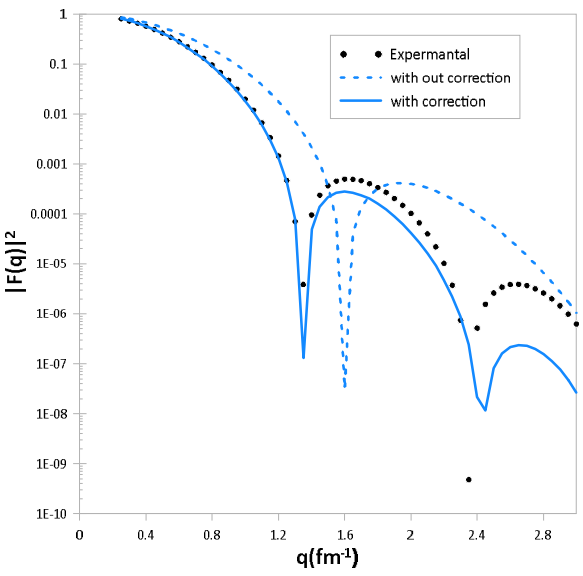

FIG. 3. The elastic form factors for the ^{28}Si nucleus.

A formula for the transition charge density given in Eq. (19) was employed to determine the inelastic longitudinal electron-scattering form factors F(q). The OXBASH code was used to calculate OBDM elements required for evaluating the form factors of open-shell nuclei. The model-space transition density was determined using Eq. (17) [22], with the interaction matrix elements taken from the USDB (Universal sd-shell B) interaction for 2s-1d shell nuclei [23]. The theoretical determination of the proportionality constant N does not involve any adjustable parameters. In this section, the computed longitudinal Coulomb C2 form factors are presented as functions of the momentum transfer q for the transitions with an observed Ex = 1.78MeV [24] and experimental value of B(C2) = 415 $e^2.fm^4$ for ^{28}Si, and observed Ex = 2.237 MeV [25] with an experimental value of B(C2) = 235 $e^2.fm^4$ for ^{32}S.

Figures 5 and 6 illustrate the calculated and experimental results. The blue dashed curves represent the model-space contributions, which include configuration mixing. The blue dash-dotted curves correspond to the core-polarization contributions, which account for two-body effects. The solid blue curves show the total calculated form factors obtained by combining the model-space and core-polarization components. The experimental data are shown as black dotted symbols (•). The results demonstrate that the experimental data cannot be reproduced using the model-space contributions alone, as these underestimate the measured values across the full momentum transfer range. However, when both the model-space effects and the core-polarization contributions are included, the calculated longitudinal C2 form factors show excellent agreement with the experimental data for all momentum transfer values q.

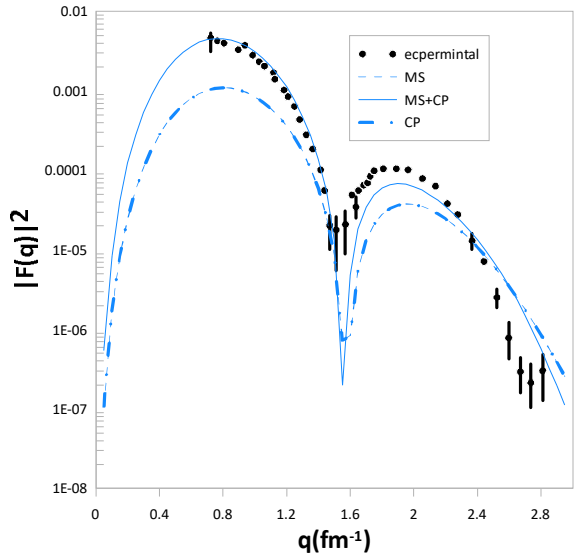

FIG. 6. The inelastic longitudinal C2 form factors for the ^{32}S nucleus.

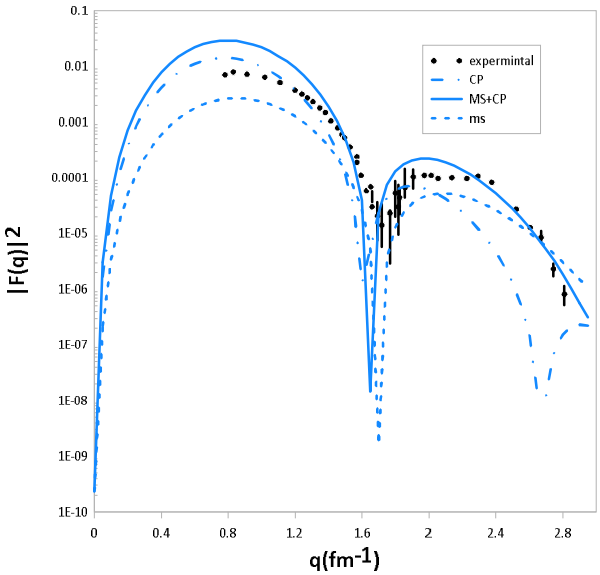

FIG. 5. The inelastic longitudinal C2 form factors for the ^{28}Si nucleus.

Figure 7 illustrates the inelastic longitudinal Coulomb C4 form factors of the ^{28}Si nucleus. The calculated longitudinal Coulomb C4 form factors are depicted in relation to the momentum transfer q for the transitions with an observed excitation energy of 4.617 MeV. The experimental B(C4) of the above nuclei is 27 500 e^2fm^4 [24]. In this figure, the blue dashed shapes symbolize the influence of the model space in ^{28}Si, adjusted for configuration mixing. The blue dash-dotted shape symbolizes the core polarization investment, which is adjusted for the effect of two bodies. The solid blue shape symbolizes the overall investment, obtained by combining the model-space and core-polarization contributions for ^{28}Si.

Figure 8 illustrates the inelastic longitudinal Coulomb C2 and C4 form factors of the ^{32}S nucleus. The calculated longitudinal C2 and C4 form factors are depicted in relation to the momentum transfer q for the transitions. For the $0^+ \rightarrow 2_2^+$ and $0^+ \rightarrow 4_1^+$ for ^{32}S with observed excitation energies of 4.282 MeV and 4.46 MeV, respectively. The experimental values of B(C2) and B(C4) of the above nuclei are 68.8, 50700 (e^2fm^4) [25]. In this figure, the blue dash shapes symbolize the influence of the C2, the blue dash-

dotted shapes symbolize C4, which includes both contributions of the model space and core polarization effect, adjusted for the effect of two bodies. The blue solid shapes symbolize the overall investigated data, calculated by combining the C2 and C4 for ^{32}S. The black (•) "dotted symbols" are the experimental data. These figures demonstrate that the model-space contribution alone cannot accurately reproduce the experimental data across the full range of momentum transfer q. However, when the effects of core polarization are incorporated, the calculated longitudinal Coulomb C4 form factors show good agreement with the experimental data throughout the entire momentum transfer range, as indicated by the solid curves.

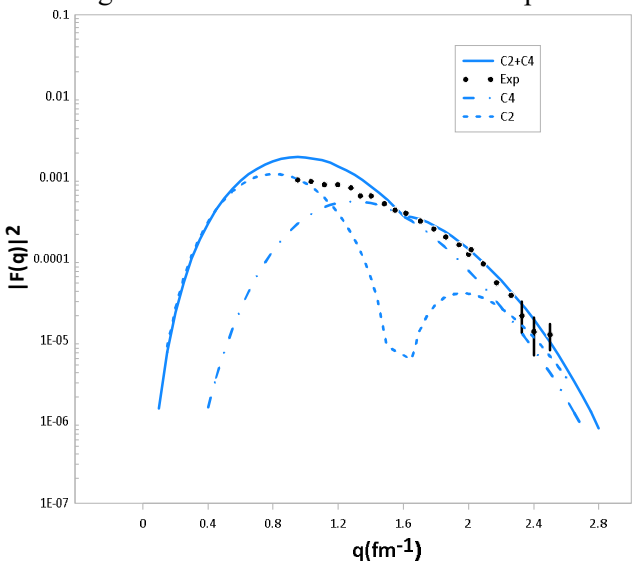

FIG. 8. Illustration of the inelastic longitudinal (C2+C4) form factors For ^{32}S nucleus.

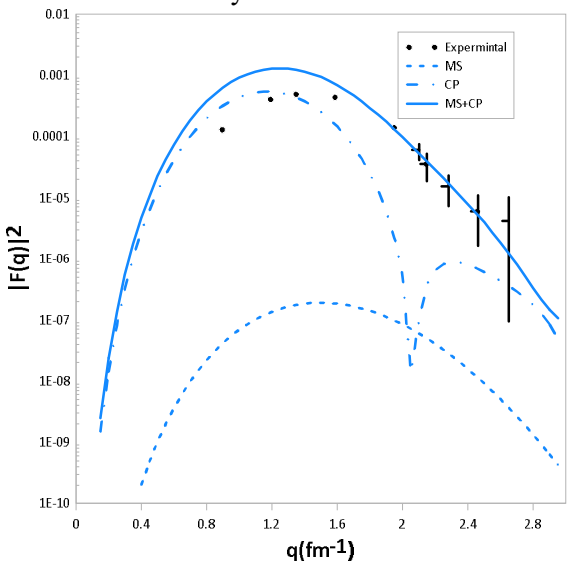

FIG. 7. Illustration of the inelastic longitudinal C4 form factors For ^{28}Si nucleus.

4. Conclusions

Based on the obtained results, we draw the following conclusions:

1. Considering the effects of the center of mass, Pauli pair correlation functions, and higher occupation probabilities is generally crucial to achieving strong agreement between the calculated charge density distributions and the experimental data for the ^{28}Si and ^{32}S nuclei.
2. The fixed characteristics and energy levels can be accurately described by the sd-shell models. However, these models are less effective in characterizing dynamical characteristics, including the rates of C2 and C4 transitions and the form factors of electron scattering.
3. The core-polarization impact improves the form factors and brings the mathematical predictions of the longitudinal form factors closer to the experimental data in the C2 and C4 transitions, which is the subject of this study.

References

[1] de Forest, T. and Walecka, J.D., Adv. Phys., 15 (1966) 1.

[2] Walecka, J.D., Nucl. Phys. A, 574 (1994) 271.

[3] Brown, B.A., Radhi, R., and Wildenthal, B.H., Phys. Rep., 101 (5) (1983) 313.

[4] Radhi, R.A., Alzubadi, A.A., and Rashed, E.M., Nucl. Phys. A, 947 (2016) 12.

[5] Mahmood, L.A. and Flaiyh, G.N., Iraqi J. Sci., 57 (2016) 1742.

[6] Mahmood, L.A. and Flaiyh, G.N., Iraqi J. Phys., 14 (2016) 129.

[7] Sarriguren, P. and Merino, D., Phys. Rev. C, 99 (2019) 034325.

[8] Al-Rahmani, A.A., Fadhil, S.N., and Hamoudi, A.K., Iraqi J. Sci., 22 (2024) 1357.

[9] Flaiyh, G.N. and Sharrad, F.I., Iran. J. Sci. Technol., Trans. A: Sci., 42 (2018) 2323.

[10] Ahmad, I., J. Phys. G: Nucl. Part. Phys., 20 (3) (1994) 507.

[11] Bergstrom, J., Kowalski, S., and Neuhausen, R., Phys. Rev. C, 25 (1982) 1156.

[12] Brown, B.A., Wildenthal, B.H., Williamson, C.F., Rad, F.N., Kowalski, S., Crannell, H., and O'Brien, J.T., Phys. Rev. C, 32 (1985) 1127.

[13] Ahmad, I. and Auger, J.P., Nucl. Phys. A, 352 (1981) 425.

[14] Benson, H.G. and Flowers, B.H., Nucl. Phys. A, 126 (1969) 305.

[15] Walecka, J.D., "Electron Scattering for Nuclear and Nucleon Structure", (Cambridge University Press, Cambridge, 2001).

[16] Donnelly, T.W. and Sick, I., Rev. Mod. Phys., 56 (1984) 461.

[17] Brussard, P.J. and Glaudemans, P.W.M., "Shell-Model applications in Nuclear Spectroscopy", (North Holland, Amesterdam, 1977).

[18] Tassie, L.J., Aust. J. Phys., 9 (1956) 407.

[19] Hassani, S., "Mathematical Physics: A Modern Introduction to Its Foundations", 2nd Ed., (Cham: Springer International Publishing, 2013), chapter 15, p.482.

[20] De Vries, H., De Jager, C.W., and De Vries, C., At. Data Nucl. Data Tables, 36 (1987) 495.

[21] Fricke, G., Bernhardt, C., Heilig, K., Schaller, L.A., Schellenberg, L., Shera, E.B., and Dejager, C.W., At. Data Nucl. Data Tables, 60 (1995) 177.

[22] Brown, B.A., Et Chegoyen, A., Godwin, N.S., Rae, W.D.M., Richter, W.A., Warburton, W.E., Winfield, J.S., Zhao, L., and Zimmerman, C.H., MSU- NSCL Rep. No. 1289, (2005).

[23] Brown, B.A. and Richter, W.A., Phys. Rev. C, 74 (2006) 34315.

[24] Li, G.C., Yearian, M.R., and Sick, I., Phys. Rev. C, 9 (1974) 1861.

[25] Wildenthal, B.H., Brown, B.A., and Sick, I., Physical Review C, 32 (1985) 2185.